

CO and HCN observations of carbon stars*

M.A.T. Groenewegen¹, F. Baas², T. de Jong^{3,4}, and C. Loup¹

¹ Institut d'Astrophysique de Paris, CNRS, 98 bis Boulevard Arago, F-75014 Paris, France

² Joint Astronomy Centre, 660 N. A'ohoku Place, University Park, Hilo, HI 96720, USA

³ Astronomical Institute 'Anton Pannekoek', Kruislaan 403, 1098 SJ Amsterdam, The Netherlands

⁴ Space Research Groningen, P.O. Box 800, 9700 AV Groningen, The Netherlands

Received 23 March 1995 / Accepted 12 June 1995

Abstract. We present CO and HCN observations of carbon stars. They consist of partly new detections in the ^{12}CO J = (1-0), (2-1) and HCN(1-0) lines obtained with the SEST and the IRAM telescope, and of ^{12}CO and ^{13}CO J = (1-0), (2-1) and (3-2) observations with IRAM and the JCMT of some of the infrared brightest carbon stars.

Recently, Bujarrabal et al. (1994a,b) proposed a critical value for the ratio of the integrated intensities HCN(1-0)/ ^{12}CO (1-0) to distinguish between carbon stars and oxygen-rich stars. In four carbon stars we find ratios consistent with their borderline value, and in two cases HCN/CO ratios below their suggested borderline value in stars which are almost certainly carbon stars. The apparent discrepancy may lie in the fact that the critical line ratio in Bujarrabal et al. is derived for the 30m IRAM telescope, while our ratios are derived from 15m SEST data. The difference in beam size may result in slightly different excitation regions being sampled.

Key words: circumstellar matter – stars: mass loss – stars: AGB; carbon – radio lines: stars

1. Introduction

Millimeter observations of molecules in the circumstellar envelopes (CSEs) around AGB stars allow the study of several interesting aspects of AGB evolution: the mass loss rate and the mass loss history of the central star, the chemistry in CSEs and the evolutionary status of the star.

The CO molecule is an excellent tracer of the mass loss rate (history) since it is very stable and the most abundant molecule

Send offprint requests to: M. Groenewegen

* The James Clerk Maxwell Telescope is operated by the Observatories on behalf of the Science and Engineering Council of the United Kingdom, the Netherlands Organization for Scientific Research, and the National Research Council of Canada. Based on observations collected at the European Southern Observatory, La Silla, Chile.

apart from H_2 . This means that CO is observable in a large number of stars (the CO+HCN catalog of Loup et al. 1993 (hereafter L93) contains data on 444 sources) and traces the mass loss rate history up to several 10^3 yrs ago (e.g. Van der Veen & Olofsson 1990).

The chemistry in the CSEs has been studied best in two stars that are very close by and therefore allow the detection of less abundant species: the oxygen-rich and carbon-rich archetypes OH 231.8+4.2 and IRC +10 216 (CW Leo). About 50 different circumstellar molecular species were detected up to 1992 (Olofsson 1993).

One indicator of the evolutionary status of carbon stars is the $^{12}\text{C}/^{13}\text{C}$ ratio. In most giants, after the first dredge-up, this ratio is about 20 (e.g. Charbonnel 1994). On the AGB, due to possible consecutive (third) dredge-ups, this ratio is expected to be higher. On the other hand, there are peculiar carbon stars with $^{12}\text{C}/^{13}\text{C}$ in the range 3-5 (e.g. Y CVn or RY Dra, see e.g. Jura et al. 1988). For carbon stars where there are no optical or infrared high-resolution spectra available, the $^{12}\text{CO}/^{13}\text{CO}$ ratio may be used to estimate the $^{12}\text{C}/^{13}\text{C}$ ratio.

In this paper we present CO and HCN observations of a sample of carbon stars. On the one hand of carbon stars which, at the time of observation (1991), had not been observed previously in CO (or either only the (1-0) or (2-1) line), and on the other hand of a sample of infrared-bright carbon stars for which we obtained high-quality ^{12}CO and ^{13}CO J = (1-0), (2-1) and, for some, (3-2) observations.

In Sect. 2. the sample is described. The observations are outlined in Sect. 3 and the results are discussed in Sect. 4.

2. The sample

The carbon stars which we observed can be separated into two groups: (1) a sample which will be denoted the 'new sample' which consists of infrared-bright ($S_{12} > 100$ Jy) carbon stars taken (except 2 stars) from the list of Groenewegen et al. (1992) for which there were no CO measurements available at the time of the observation in 1991 (or either only the (1-0) or (2-1) line), and (2) a sample which will be denoted the 'well-known sample'

which consists of some of the (infrared and CO) brightest carbon stars observable from the northern hemisphere.

Two stars in the new sample (IRAS 12419–6058 and IRAS 18464–0656) are included as possible carbon stars. Their LRS spectra are more or less featureless, similar to some known extremely red carbon stars (Groenewegen et al. 1992, Omont et al. 1993). These two stars have no $3.1 \mu\text{m}$ absorption feature due to HCN and C_2H_2 , but dust emission may have filled in the feature (Groenewegen et al. 1994). The location of these stars in a $[K-L]$, $[12-25]$ color-color diagram (for a discussion on the usefulness of this particular color-color diagram see Epchtein et al. 1990) suggest that they are indeed carbon stars (see the discussion in Groenewegen et al. 1994 and Sect. 4.2).

For the new sample the aim of the observations was to detect CO and HCN, in order to derive rough estimates of the mass loss rates and obtain the expansion velocities of the envelopes. For the well-known sample we aimed at obtaining high-quality data, to be modeled in detail in a forthcoming paper with a molecular and dust radiative transfer model. In Table 1, basic data of the stars that were observed are listed, together with references to previous observations. Coordinates for the stars in the well-known sample are relatively well documented. Most of the coordinates of the stars in the new sample are taken from the IRAS PSC. Some of the coordinates of AFGL sources are taken from Allen et al. (1977), Joyce et al. (1977), Grasdalen et al. (1983), or averages were taken. The coordinates of 18041–3317 are from Fuenmayor (1981; star 272)

3. The observations

The observations were obtained with the SEST at La Silla, Chile, the IRAM telescope at Pico Veleta, Spain, and the JCMT on Mauna Kea, Hawaii.

The SEST data were taken between March 24–26, 1991. We used two Schottky receivers with the wide band AOS backend. The main-beam efficiencies and HPBW (half-power beam-width) at 88.6 (HCN(1-0)), 115.3 (CO(1-0)) and 230.5 (CO(2-1)) GHz were 0.76 ($56''$), 0.71 ($44''$) and 0.50 ($23''$), respectively. The velocity resolution at 115 GHz was 1.81 km s^{-1} . The CO(2-1) data were smoothed to give the same resolution. The pointing was found to be accurate within $10''$. Calibration was done by a standard chopping wheel technique, switching between the sky and an ambient load. Linear baselines were subtracted. The spectra were obtained using dual beam switch mode with a throw of $11.5'$.

The IRAM observations were obtained between 7–10 August, 1991. We used two SIS receivers with two $512 \times 1 \text{ MHz}$ filter banks as backend. The $^{12}\text{CO}(1-0)$ and $^{12}\text{CO}(2-1)$, c.q. the $^{13}\text{CO}(1-0)$ and $^{13}\text{CO}(2-1)$ transitions, were observed simultaneously. We used the wobbler with a throw of $120''$ in azimuth. The half-power beam width and main-beam efficiencies were $21''$, 0.60 and $12.5''$, 0.45 for the $J = 1-0$ and $2-1$ transition, respectively. Linear baselines were removed and the observed line intensities were calibrated using sources in the list of Mauersberger et al. (1989). The (2-1) data were smoothed to give a uniform velocity resolution of $\sim 2.6 \text{ km s}^{-1}$ for both transitions.

The JCMT $^{12}\text{CO}(3-2)$ and $^{13}\text{CO}(3-2)$ spectra were taken on July 10, 13 and 15, 1992, in beam switch mode with receiver B3i which has a mean beam efficiency of 0.53. The chop frequency was 1 Hz and the chop throw was $120''$ in azimuth. The beam width (FWHM) was $14.3''$. The backend was the AOSC (an acousto-optical spectrometer) with a resolution of 0.5 MHz. All data have been smoothed to an effective resolution of 2.6 km s^{-1} .

All temperatures are expressed on a main-beam temperature scale, i.e. the antenna temperature divided by the main-beam efficiency. We estimate the calibration of the SEST, IRAM and JCMT observations to be accurate to 10% (1σ). In Table 2 are listed the name of the object, the observing run, the transition, the rms noise, the peak temperature, the integrated intensity, the central velocity with respect to the local standard of rest (not for the ^{13}CO transitions) and half the velocity width at zero intensity (not for the ^{13}CO transitions) which equals the expansion velocity of the circumstellar shell. These quantities were determined either directly from the profiles or from fits to the profiles made with the reduction program CLASS (Forveille et al. 1990). Typical uncertainties in the central velocity and the expansion velocity are 1 km s^{-1} . The uncertainties in the peak temperature and the integrated intensity are dominated by the calibration uncertainties. Values flagged with a colon are particularly uncertain. The calibrated profiles are shown in Figs. 1–30. Figures 1–14 show the profiles of the stars in the new sample, usually two stars per figure and roughly in order of right ascension. Figures 15–30 show the profiles of the stars in the well-known sample, with one star per figure and in order of right ascension. Some observations are influenced by interstellar contamination. These observations are marked in Table 2 and discussed in Sect. 4.1.

4. Results

For 12 stars we provide the first detection in the ^{12}CO line. For another 17 stars we present the first detection in either the $J = 1-0$ or $2-1$ transition. We observed the HCN(1-0) line in 6 stars and detected 4 (AFGL 4183 is a tentative detection; Fig. 5), 3 of which for the first time. For many stars we present for the first time ^{13}CO data and/or $J = 3-2$ observations.

Below we comment on some individual sources.

4.1. Individual sources

4.1.1. V414 Per (Fig. 1)

In the 1-0 profile a spike can be seen at $V_{\text{LSR}} = -10 \text{ km s}^{-1}$, with a width of about 5 km s^{-1} . The spike is present in all four subscans with about equal intensity. The Galactic CO maps of Dame et al. (1987; D87) show CO emission in the direction of the Galactic coordinates of the source ($l = 157^\circ$, $b = -10.9^\circ$), but at a slightly different velocity (between -5 and $+5 \text{ km s}^{-1}$). Previous observations of the 2-1 line by Woodsworth et al. (1991) show a 'dip' at about -14 km s^{-1} (in addition to a very strong 'dip' at -3 km s^{-1}). We believe the spike to be of interstellar origin.

Table 1. The observed stars

Identification	R.A. (1950)	Dec. (1950)	Previous observations ¹
The new sample			
V414 Per	03 48 53.6	39 43 54	2-1: Woodsworth et al. (1991)
V636 Mon	06 22 38.2	-09 05 32	2-1: Zuckerman & Dyck (1989); Woodsworth et al. (1991); HCN: Lucas et al. (1988)
AFGL 1085	07 09 53.8	-20 12 24	2-1: Zuckerman & Dyck (1986a)
07373-4021	07 37 22.0	-40 21 49	1-0: Nyman et al. (1992)
AFGL 4078	07 45 25.6	-71 12 19	1-0: Nyman et al. (1992)
08074-3615	08 07 27.0	-36 15 40	1-0: Zuckerman & Dyck (1986b); HCN: Lucas et al. (1988)
09513-5324	09 51 20.8	-53 24 43	
11145-6534	11 14 33.9	-65 34 34	
11318-7256	11 31 51.4	-72 56 41	1-0: Nyman et al. (1992)
12419-6058	12 41 55.9	-60 58 45	
RU Vir	12 44 45.7	04 25 04	1-0 ⁽²⁾ : Knapp & Morris (1985), Nyman et al. (1992); HCN: Lucas et al. (1988)
AFGL 4183	13 47 47.3	-65 31 56	
AFGL 4202	14 48 25.0	-61 52 05	
16079-4812	16 07 54.9	-48 12 09	
17446-4048	17 44 40.9	-40 48 37	1-0: Nyman et al. (1992)
AFGL 5416	17 53 20.0	-30 30 25	1-0: Zuckerman & Dyck (1986b)
AFGL 5440	18 03 38.5	-23 44 42	
18041-3317	18 04 11.4	-33 16 58	
AFGL 2096	18 11 59.6	-22 44 59	
AFGL 2118	18 15 37.0	-06 53 06	
AFGL 2154	18 23 57.4	-06 55 54	1-0: Zuckerman et al. (1986)
AFGL 2256	18 46 28.6	-06 56 33	2-1: Volk et al. (1993)
AFGL 2333	19 07 34.0	09 21 56	2-1: Volk et al. (1993)
AFGL 2513	20 07 15.0	31 16 52	HCN: Zuckerman & Dyck (1986b), Lucas et al. (1988)
U Cyg	20 18 03.2	47 44 09	1-0, 2-1: Olofsson et al. (1993b)
AFGL 2604	20 31 09.0	42 22 24	
The well-known sample			
AFGL 67	00 24 47.0	69 22 16	1-0, HCN: L93
AFGL 190	01 14 26.3	66 58 05	2-1, HCN: L93; Volk et al. (1993)
IRC +50 096	03 22 59.1	47 21 22	1-0, HCN: L93; Knapp & Chang (1985), Sopka et al. (1989)
AFGL 865	06 01 17.4	07 26 06	1-0, 2-1, HCN: L93; Knapp & Chang (1985), Bujarrabal et al. (1994b)
CW Leo	09 45 14.9	13 30 41	1-0, 2-1, HCN: L93; Kahane et al. (1992), Williams & White (1992), Avery et al. (1992), Bujarrabal et al. (1994b), Groesbeek et al. (1994)
CIT 6	10 13 10.9	30 49 17	1-0, 2-1, HCN: L93; Kahane et al. (1992), Bujarrabal et al. (1994b)
V Hya	10 49 11.3	-20 59 05	1-0, 2-1, HCN: L93; Jura et al. (1988), Olofsson et al. (1993b), Bujarrabal et al. (1994b)
Y Cvn	12 42 47.1	45 42 48	1-0, 2-1, HCN: L93; Jura et al. (1988), Bujarrabal et al. (1994b)
RY Dra	12 54 28.1	66 15 52	1-0, 2-1, HCN: L93; Jura et al. (1988)
AFGL 1922	17 04 54.6	-24 40 39	1-0, 2-1, HCN: L93
V Aql	19 01 44.0	-05 45 38	1-0, 2-1, HCN: L93
AFGL 2477	19 54 49.2	30 35 54	1-0, 2-1, HCN: L93
AFGL 2494	19 59 24.8	40 47 18	1-0, 2-1, HCN: L93; Volk et al. (1993)
S Cep	21 35 52.7	78 23 59	1-0, 2-1, HCN: L93; Bujarrabal et al. (1994b)
AFGL 3068	23 16 42.4	16 55 10	1-0, 2-1, HCN: L93; Sopka et al. (1989), Bujarrabal et al. (1994b), Volk et al. (1993)
LP And	23 32 01.3	43 16 27	1-0, 2-1, HCN: L93; Knapp & Chang (1985), Bujarrabal et al. (1994b)

Notes. (1) If more than one CO measurement is reported in the literature, or also HCN data, reference is made to the ¹²CO+HCN catalog of L93. Data on ¹²CO transitions J=3-2 or higher, or ¹³CO data, are explicitly referred to. Data not included in L93 are also referred to. The references for CW Leo include only the most recent ones. (2) For both cases the peak temperature was less than 3 times the rms noise.

Table 2. The observed quantities

name	run ¹	transition ²	rms (K)	T_{peak}^3 (K)	$\int T \, dv$ (K km s ⁻¹)	v_c (km s ⁻¹)	v_e (km s ⁻¹)	remarks
The new sample								
V414 Per	2	12/1-0	0.02	0.23	13.7 ⁴	-27.0	30.7	
	2	12/2-1	0.06	0.75	39.0	-25.5	30.7	
V636 Mon	1	12/1-0	0.04	0.22	5.8(:)	10.9	20(:)	
	1	12/2-1	0.12	0.8	26	9.1	20(:)	
AFGL 1085	1	12/1-0	0.03	0.11	4.0	9.7	24.5	interstellar contamination
07373-4021	1	12/1-0	0.10		<5			
	1	12/2-1	0.20	0.7	14	20(:)	18.6(:)	
AFGL 4078	1	12/1-0	0.04	0.65	13.0	-36.3	14.0	
	1	12/2-1	0.2	3.5	64.1	-36.7	13.0	
08074-3615	1	12/1-0	0.04	0.23	5.5	9.8	21.7	
	1	12/2-1	0.11		<9			
	1	HCN	0.01	0.08	1.3	14.2	15.3(:)	
09513-5324	1	12/1-0	0.04	0.38	9.6	-8.5	20.9	
	1	12/2-1	0.12	0.45	12.4	-10.0	19.0	
11145-6534	1	12/1-0	0.03	0.24	6.5	-24	18.5	interstellar contamination
	1	12/2-1	0.11		<14			
11318-7256	1	12/1-0	0.03	0.18	6.7	-6	28	
	1	12/2-1	0.08	0.55	20	2	25	
	1	HCN	0.03	0.22	8.8	0	25	
12419-6058	1	12/1-0	0.03	0.16	4(:)	-60(:)	22(:)	interstellar contamination
	1	HCN	0.016		<1			
RU Vir	2	12/1-0	0.03	0.77	19.7	-1.1	15.2	
	2	13/1-0	0.04		<2			
	2	12/2-1	0.10	2.0	49.6	-0.8	15.6	
	2	13/2-1	0.08		<3			
AFGL 4183	1	12/1-0	0.04	0.36	9.4	-44	18.5	
	1	12/2-1	0.13	0.70	13.5	-45	14.2	
	1	HCN	0.012	0.05	0.8(:)	-40		
AFGL 4202	1	12/1-0	0.05	0.63	16.5	25.3	19.0	
	1	12/2-1	0.16	1.15	29.6	23.4	19.0	
16079-4812	1	12/1-0	0.06	0.39	8.9	-41.7	14.5(:)	interstellar contamination
	1	12/2-1	0.10	0.86	16.8	-43.5	14.5(:)	interstellar contamination
17446-4048	1	12/1-0	0.04	0.59	13.0	0.0	17.0	
	1	13/1-0	0.04		<1.5			
	1	12/2-1	0.14	0.76	18.2	4.0	16.3	
AFGL 5416	1	12/1-0	0.04	0.24	5.1 ⁴	-11	19(:)	interstellar contamination
	1	12/2-1	0.09	0.90	19.8	-5	19(:)	interstellar contamination
	1	HCN	0.01	0.03	0.4(:)	-10		
AFGL 5440	2	12/1-0	0.04	1.5	15.6	21.2	22.5	
	2	12/2-1	0.07	1.8	23.0	24.2	20.9	
18041-3317	1	12/1-0	0.03	0.12	3.1(:)	80(:)	19(:)	tentative detection
AFGL 2096	2	12/1-0	0.03	0.2	5.0	21.3	18.0	
	2	12/2-1	0.07	0.6	23.0	24.2	17.6	
AFGL 2118	2	12/1-0	0.03	0.35	11.8	23.1	20.5	
	2	13/1-0	0.02		<2			
	2	12/2-1	0.07	0.8	24.6	24.4	19.3	
	2	13/2-1	0.04		<2.5			
AFGL 2154	1	12/1-0	0.03	0.3	9(:)	1.8	30(:)	interstellar contamination
	1	12/2-1	0.09	0.34	8.2(:)	-1.0	27(:)	
AFGL 2256	1	12/1-0	0.05	0.13	3.8	59.8	15.4	
	1	HCN	0.02		<1.0			

Table 2. (continued)

name	run ¹	transition ²	rms (K)	T_{peak}^3 (K)	$\int T \, dv$ (K km s ⁻¹)	v_c (km s ⁻¹)	v_e (km s ⁻¹)	remarks
AFGL 2333	2	12/1-0	0.02	1.5	36(:)	44(:)	18(:)	interstellar contamination
	2	12/2-1	0.05	2.6	58(:)	45(:)	20(:)	interstellar contamination
AFGL 2513	2	12/1-0	0.02	0.6	15.7	17.7	26.2	interstellar contamination
	2	12/2-1	0.04	1.4	49.5	17.9	25.0	
U Cyg	2	12/1-0	0.02	0.42	8.9	25.0	14.1	
	2	13/1-0	0.02		<1.5			
	2	12/2-1	0.05	1.1	22.9	25.6	14.3	
	2	13/2-1	0.04		<4			
AFGL 2604	2	12/1-0	0.04	0.2	4.5	24.7	13.1	interstellar contamination
	2	12/2-1	0.13	0.85	16.5	25.1	13.1	
The well-known sample								
AFGL 67	2	12/1-0	0.03	1.3	35.3	-28.2	17.6	
	2	13/1-0	0.06	0.08	1.8			
	2	12/2-1	0.06	2.7	64.9	-27.5	16.8	
	2	13/2-1	0.04	0.15	3.6			
	3	12/3-2	0.20	2.0	47.1	-22.9	18.4	
AFGL 190	3	13/3-2	0.08		<4			
	2	12/1-0	0.03	1.3	33.6	-39.4	18.0	
	2	13/1-0	0.02		<2			
	2	12/2-1	0.10	3.5	80.0	-39.2	18.0	
	2	13/2-1	0.04	0.14	3.6			
IRC +50 096	3	12/3-2	0.15	1.5	30.7	-41.0	18.4	
	2	12/1-0	0.03	1.95	49.1	-16.5	15.2	
	2	13/1-0	0.02	0.10	3.7			
	2	12/2-1	0.10	5.4	117.1	-16.2	14.8	
	2	13/2-1	0.03	0.2	7.4			
AFGL 865	3	12/3-2	0.05	2.7	52.8	-17.8	16.4	
	3	13/3-2	0.09	0.21	6.4			
	2	12/1-0	0.04	2.2	50.7	42.9	16.4	
	2	13/1-0	0.02	0.12	3.4			
	2	12/2-1	0.10	4.2	83.8	43.3	16.8	
CW Leo	2	13/2-1	0.04	0.22	7.2			
	3	12/3-2	0.09	1.5	28.3	41.7	16.4	
	2	12/1-0	0.03	16.2	431	-25.9	15.4	
	2	13/1-0	0.04	0.9	42.1			
	2	12/2-1	0.06	38.7	878	-25.5	15.4	
CIT 6	2	13/2-1	0.09	3.5	128			
	3	12/3-2	0.16	41.6	889.9	-28.1	16.4	
	3	13/3-2	0.20	3.8	125.1			
	2	12/1-0	0.03	4.0	128	-1.6	17.6	
	2	13/1-0	0.02	0.15	7.4			
V Hya	2	12/2-1	0.06	8.4	230	-1.0	17.2	
	2	13/2-1	0.05	0.35	16.5			
	3	12/3-2	0.16	6.6	162.9	-2.2	19.3	
	3	13/3-2	0.09	0.46	17.7			
	2	12/1-0	0.04	2.1	41.6	-14	27	
V Hya	2	13/1-0	0.05		<5			
	2	12/2-1	0.07	3.9	78.8	-13.9	30	
	2	13/2-1	0.19		<25			

Table 2. (continued)

name	run ¹	transition ²	rms (K)	T_{peak} ³ (K)	$\int T dv$ (K km s ⁻¹)	v_c (km s ⁻¹)	v_e (km s ⁻¹)	remarks
Y CVn	2	12/1-0	0.03	0.73	9.9	21.4	9.8	
	2	13/1-0	0.02	0.32	4.3			
	2	12/2-1	0.09	1.8	23.3	21.1	9.8	
	2	13/2-1	0.03	0.44	6.1			
RY Dra	2	12/1-0	0.03	0.32	5.7	-5.1	10.9	
	2	13/1-0	0.03	0.24	3.9			
	2	12/2-1	0.09	0.75	23.3	-5.0	10.7	
	2	13/2-1	0.05	0.34	6.0			
AFGL 1922	2	12/1-0	0.05	1.9	51.9	-4.3	19.3	
	2	13/1-0	0.03	0.2	5.9			
	2	12/2-1	0.10	3.2	80.8	-3.9	21.7	
	2	13/2-1	0.05	0.28	9.0			
V Aql	2	12/1-0	0.03	0.6	8.0	54.0	9.4	
	2	13/1-0	0.02		<1.1			
	2	12/2-1	0.06	1.5	20.6	54.0	11.5	
	2	13/2-1	0.03		<1.1			
AFGL 2477	2	12/1-0	0.05	1.18	35.7	5.9	21.3	
	2	13/1-0	0.03	0.16	5.20			
	2	12/2-1	0.11	2.8	78.1	5.5	23.3	
	2	13/2-1	0.04	0.36	10.4			
AFGL 2494	3	12/3-2	0.11	1.4	38.6	8.3	24.2	
	2	12/1-0	0.04	1.4	47.3	29.5	20.0	
	2	13/1-0	0.02	0.05	1.2(:)			
	2	12/2-1	0.07	3.5	107.1	29.4	20.9	
	2	13/2-1	0.03	0.10	2.0(:)			
	3	12/3-2	0.10	1.7	49.5	29.0	23.8	
S Cep	3	13/3-2	0.07		<4			
	2	12/1-0	0.04	0.7	33.2	-15.4	23.3	
	2	13/1-0	0.03		<2.8			
	2	12/2-1	0.08	1.8	70.7	-15.7	21.7	
AFGL 3068	2	13/2-1	0.05		<4.8			
	2	12/1-0	0.03	3.7	78.3	-30.8	15.0	
	2	13/1-0	0.02	0.42	11.0			
	2	12/2-1	0.08	8.7	158	-30.7	15.2	
	2	13/2-1	0.05	1.4	33.4			
	3	12/3-2	0.10	5.3	94.3	-30.7	16.4	
LP And	3	13/3-2	0.08	1.2	25.2			
	2	12/1-0	0.03	4.0	90.0	-17.0	14.8	
	2	13/1-0	0.02	0.27	9.4			
	2	12/2-1	0.08	7.4	150	-16.8	14.5	
	2	13/2-1	0.05	0.6	16.2			
	3	12/3-2	0.20	5.5	103.6	-17.7	15.6	
3	13/3-2	0.08	0.47	12.2				

Notes. (1) The SEST-run is labeled as 1, the IRAM-run as 2, and the JCMT-run as 3. (2) The label is x/y , where x indicates whether the data refers to the ¹²CO or ¹³CO molecule and y to the transition. (3) Peak temperature, or, for double-peaked profiles, the temperature at the line center. (4) excluding the spike.

Our J = 2-1 spectrum is of higher quality than that obtained by Woodsworth et al. (1991) with the JCMT telescope. The ratio of the integrated intensities (5.1) is close to the expected value of 4, based on the square of the ratio of the telescope diameters. The star has the highest expansion velocity of all observed objects (see the discussion in Sect. 4.3).

4.1.2. 07373-4021 (Fig. 2)

We detected the 2-1 line in this star but not the 1-0 transition. Previously, the 1-0 transition has been detected by Nyman et al. (1992). Our non-detection is presumably due to the high noise level; 0.1 K rms for our observations and 0.037 K for Nyman et al. The 2-1 profile and the 1-0 profile observed by Nyman et al. peak at the same velocity, suggesting the 2-1 detection is real.

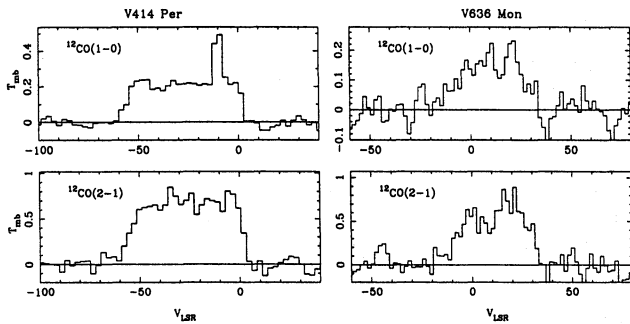


Fig. 1. V414 Per and V636 Mon

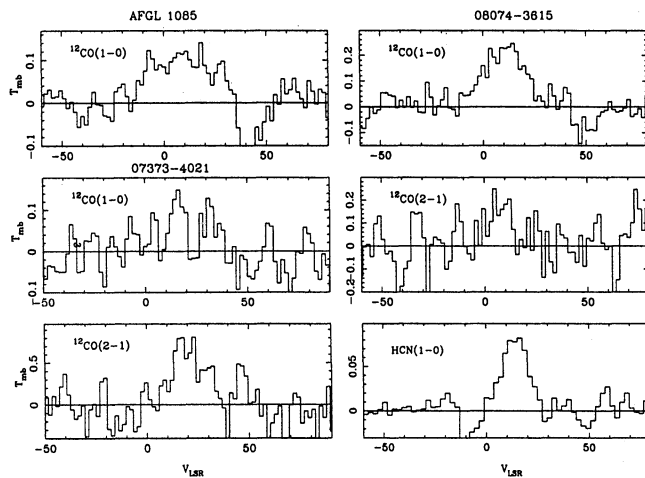


Fig. 2. AFGL 1085 (top left), 08074-3615 (right half) and 07337-4021 (bottom left)

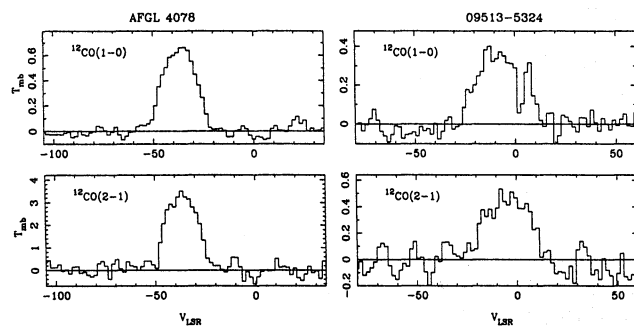


Fig. 3. AFGL 4078 and 09513-5324

4.1.3. 08074-3615 (Fig. 2)

Surprisingly, the 2-1 line is not detected while the 1-0 line is. This is most unusual as normally the 2-1 line is stronger than the 1-0 line. This could possibly be due to the uncertainty in the coordinates in combination with the smaller 2-1 beam. Zucker- man & Dyck (1986b) observed this source in the (1-0) line at a position $14''$ from ours and derived a peak temperature which, scaled to the beam width of the SEST, is 20% higher than we actually measure. This could indicate that their position is closer to the actual object; on the other hand, a difference of 20% is

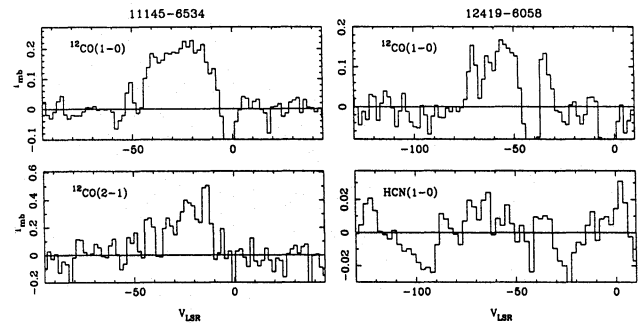


Fig. 4. 11145-6534 and 12419-6058

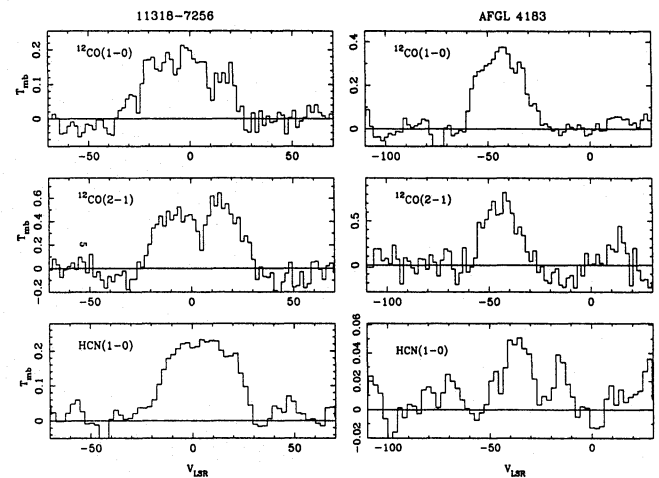


Fig. 5. 11318-7256 and AFGL 4183

well within the expected calibration uncertainties. The beam of the SEST at the frequency of the 2-1 transition is $23''$. Even if our position is off-set by $14''$, we still expect to have detected the 2-1 line.

Groenewegen (1994) gave an alternative explanation for the fact that this, and a few other sources, have 1-0 lines which are stronger than the 2-1 lines. Under special circumstances (depending on the beam size at the distance of the star, the distance at which dust shielding is effective and the size of the CO envelope) photo electric heating can raise the gas temperature in the outer layers of the circumstellar shell in such a way that the 1-0 line becomes stronger than the 2-1 line.

More detailed observations are required (in particular a small map) to eliminate the uncertainty in de coordinates and determine the location of maximum intensity. If these observations would confirm a stronger 1-0 than 2-1 line, detailed modeling is required to investigate the role of photo electric heating.

4.1.4. 12419-6058 (Fig. 4)

In the 1-0 profile an interstellar feature can be seen at $V_{\text{LSR}} = -40 \text{ km s}^{-1}$. The Galactic CO maps of D87 show CO emission in the direction of the Galactic coordinates of the source ($l = 302^\circ$, $b = +2^\circ$), at a velocity of -40 km s^{-1} . In calculating the expansion

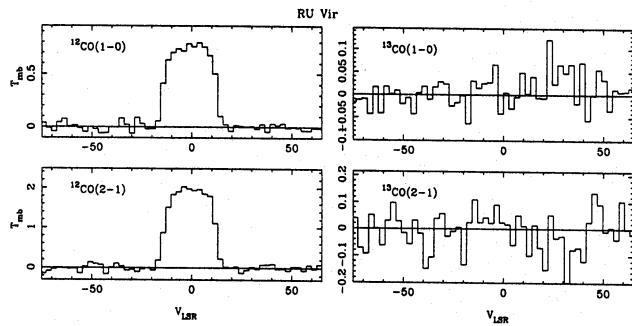


Fig. 6. RU Vir

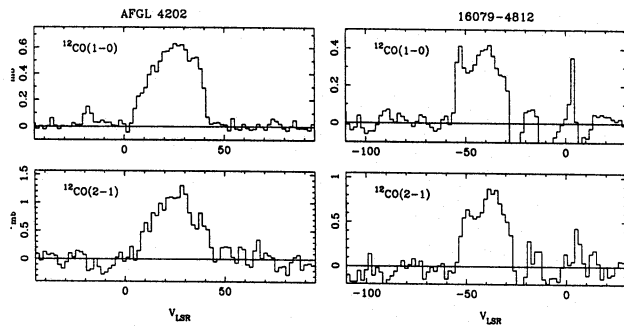


Fig. 7. AFGL 4202 and 16079-4812

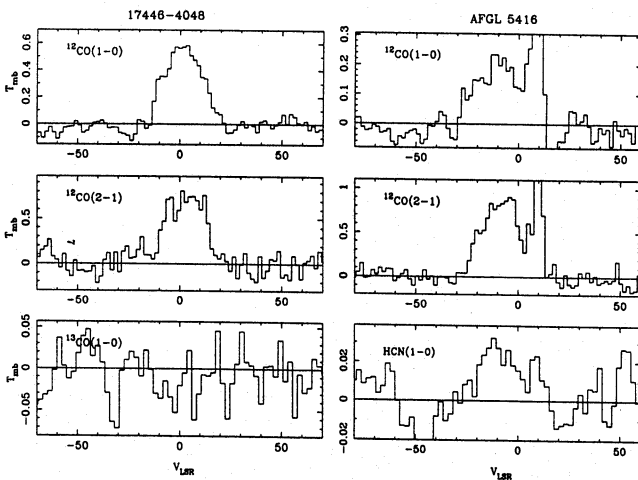


Fig. 8. 17446-4048 and AFGL 5416

velocity we assumed that the circumstellar component extends to -29 km s^{-1} .

4.1.5. IRAS 16079-4812 (Fig. 7)

In both the 1-0 and 2-1 profiles interstellar contamination is obvious near $V_{\text{LSR}} = -10$ and -25 km s^{-1} . In the direction of this source ($l = 334^\circ$, $b = +2^\circ$), interstellar contamination is possible over a wide velocity range (about -20 to -100 km s^{-1} ; D87).

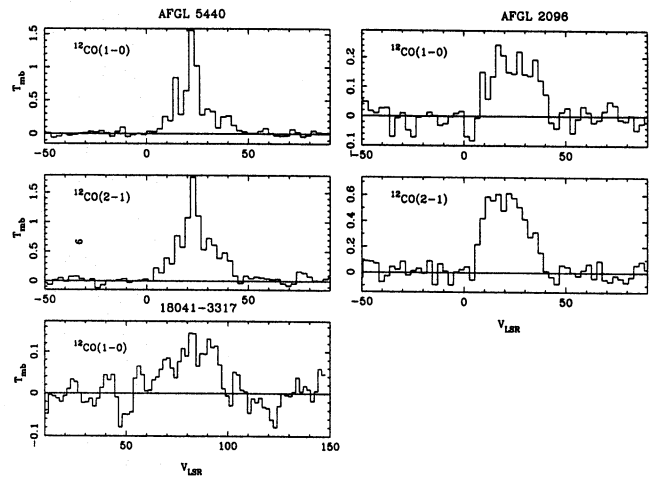


Fig. 9. AFGL 5440 (top left), 18041-3317 (bottom left) and AFGL 2096 (right hand)

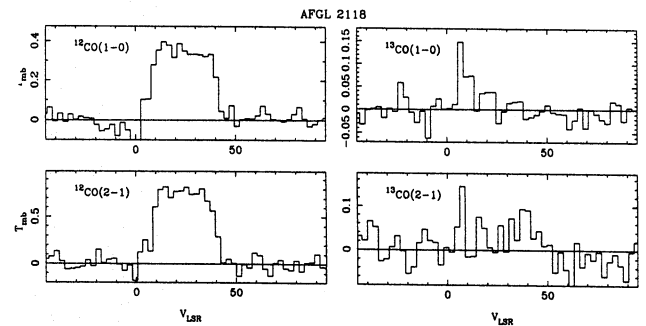


Fig. 10. AFGL 2118

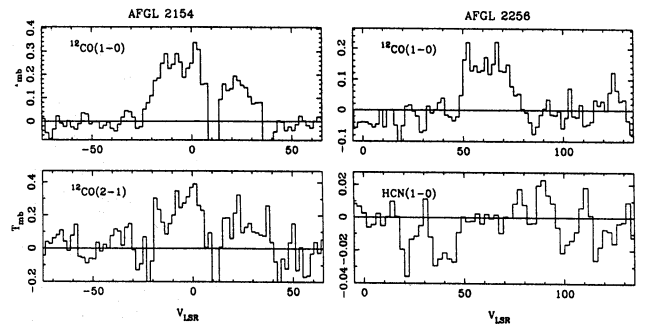


Fig. 11. AFGL 2154 and AFGL 2256

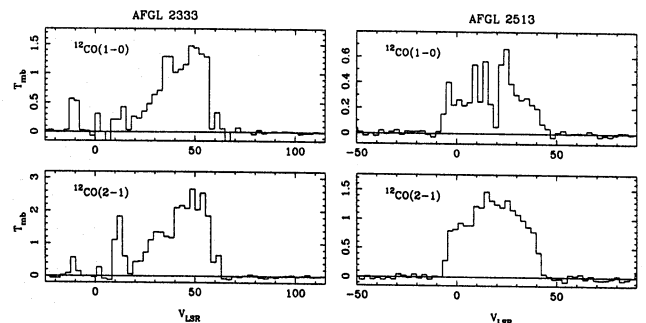


Fig. 12. AFGL 2333 and AFGL 2513

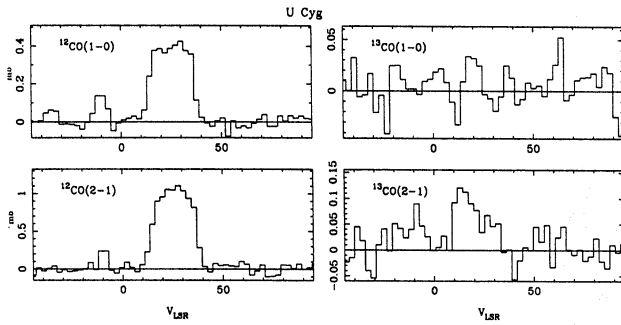


Fig. 13. U Cyg

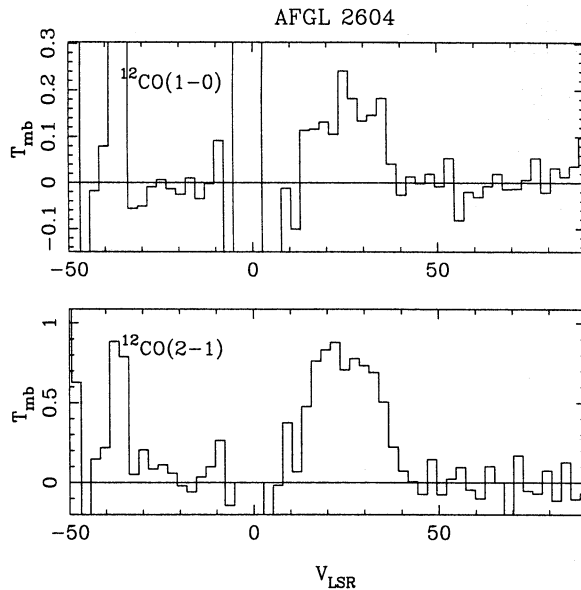


Fig. 14. AFGL 2604

4.1.6. AFGL 5416 (Fig. 8)

Interstellar contamination is visible on the red part of the CO profiles near $V_{\text{LSR}} \approx 10 \text{ km s}^{-1}$. The source is located at $l = 360^\circ$, $b = -3^\circ$ which means that interstellar contamination can occur at almost any velocity. On the other hand, the HCN profile, although noisy, is consistent with the CO data in the sense that the profiles extend from $V_{\text{LSR}} \approx -30$ to $+15 \text{ km s}^{-1}$.

4.1.7. AFGL 5440 (Fig. 9)

This object shows very unusual 1-0 and 2-1 line profiles, if real. This star is close to the Galactic center ($l = 6.9^\circ$, $b = -1.4^\circ$) and interstellar contamination may affect the profile over the velocity range from 40 to -20 km s^{-1} (D87). A small map should be made to verify this in detail.

4.1.8. AFGL 2154 (Fig. 11)

Interstellar features can be seen at velocities of 10 and 40 km s^{-1} . The Galactic CO maps of D87 show strong CO emission in the direction of the Galactic coordinates of the source ($l = 24^\circ$, b

$= +2.3^\circ$), at a velocity of 10 km s^{-1} . In calculating the expansion velocity we assumed that the circumstellar component extends from -22 to 40 km s^{-1} .

4.1.9. AFGL 2333 (Fig. 12)

The 1-0 profile and to a lesser extent also the 2-1 profile are asymmetric. This could mean that the flow is not spherically symmetric; also opacity effects could suppress the blue part of the envelope. Alternatively interstellar contamination could play a role. In this direction ($l = 43^\circ$, $b = 0^\circ$) contamination is possibly between $V_{\text{LSR}} \approx 5$ to $+75 \text{ km s}^{-1}$ (D87). Combining our observation with that of Volk et al. (1993) suggests that the peak in the 2-1 profile near $V_{\text{LSR}} = 12 \text{ km s}^{-1}$ is due to interstellar contamination and that the stellar profile extends from $V_{\text{LSR}} \approx 18$ to 65 km s^{-1} .

4.1.10. AFGL 2604 (Fig. 14)

According to D87, interstellar contamination in this direction ($l = 81^\circ$, $b = +2^\circ$) is possibly between $V_{\text{LSR}} \approx -5$ to $+20 \text{ km s}^{-1}$. This is just on the blue part of the profiles. The symmetric shape of in particular the 2-1 profile suggests that interstellar contamination probably does not affect the profiles.

4.1.11. V Hya (Fig. 21)

The atypical ^{12}CO profiles in V Hya are well documented (e.g. Tsuji et al. 1988, Kahane et al. 1988, Kahane et al. 1993). Mapping of this source has shown that the shell has a bipolar morphology superposed on a spherical component. The star possibly is a common-envelope binary system (see discussion in the references above).

4.2. The HCN observations

Bujarrabal et al. (1994a, b) presented ratios of the integrated intensities of different carbon-rich and oxygen-rich molecules to discriminate carbon-rich from oxygen-rich stars. The HCN/ ^{12}CO ratio which gives a 50% probability for a star to be carbon-rich is 0.18. A larger ratio indicates a carbon star. The ratios observed in our stars are 0.24 ± 0.03 (08074–3615), 1.3 ± 0.2 (11318–7256), <0.25 (12419–6058), 0.09 ± 0.03 (AFGL 4183), 0.07 ± 0.03 (AFGL 5416) and <0.26 (AFGL 2256). Only 11318–7256 is clearly above this limit. The other stars, for which we have little doubt in their carbon star classification, are discussed below.

The HCN/CO ratio in 08074–3615 is also above the limit of 0.18; furthermore this star is not detected in H_2O (Deguchi et al. 1989) and OH (te Lintel Hekkert et al. 1990). Its LRS spectrum is similar to other known red carbon stars (Groenewegen et al. 1992, Volk et al. 1992) and the star displays the characteristic $3.1 \mu\text{m}$ absorption feature of carbon stars (Groenewegen et al. 1994). The location of the star in the $[K - L]$, $[12 - 25]$ color-color diagram also indicates a carbon star nature (Epchtein et al. 1990, Groenewegen et al. 1994).

The HCN/CO ratio in 12419–6058 is still consistent with a carbon star nature. This star is not detected in OH (te Lintel Hekkert et al. 1990). Its LRS spectrum is similar to other known red carbon stars (Groenewegen et al. 1992, Volk et al. 1992). The star does not display the characteristic $3.1 \mu\text{m}$ absorption feature (Groenewegen et al. 1994), but the spectrum was of low S/N. Furthermore, the red colors of the object indicate that dust emission fills in, at least partly, the $3.1 \mu\text{m}$ feature (Groenewegen et al. 1994). The location of the star in the $[K - L]$, $[12 - 25]$ color-color diagram indicates a carbon star nature (Groenewegen et al. 1994).

AFGL 4183 is not detected in OH (te Lintel-Hekkert et al. 1990) and SiO (Hall et al. 1990). The star has a $3.1 \mu\text{m}$ absorption feature (Groenewegen et al. 1994) and the location in the $[K - L]$, $[12 - 25]$ color-color diagram also indicates a carbon star nature (Groenewegen et al. 1994). The LRS classification is O4, but the spectrum clearly shows a silicon carbide feature. The star is a carbon star despite its low HCN/CO ratio.

AFGL 5416 is not detected in SiO (Haikala 1990) and OH (Gaylard et al. 1989, te Lintel Hekkert et al. 1990, Le Squeren et al. 1992). Its LRS spectrum is similar to other known red carbon stars (Groenewegen et al. 1992, Volk et al. 1992, Omont et al. 1993). No infrared photometry appears to have been published for this source, so it can not be placed in the $[K - L]$, $[12 - 25]$ color-color diagram. The star is probably a carbon star despite its low HCN/CO ratio.

The HCN/CO ratio in AFGL 2256 is still consistent with a carbon star character. The star is not detected in OH (Le Squeren et al. 1992). The location in the $[K - L]$, $[12 - 25]$ color-color diagram supports a carbon star nature (Groenewegen et al. 1994). Its LRS spectrum is featureless and similar to that of known red carbon stars (Groenewegen et al. 1992, Volk et al. 1992, Omont et al. 1993). Groenewegen et al. (1994) did not detect the $3.1 \mu\text{m}$ absorption feature but the star is so red that dust emission may have at least partly filled in the feature. Kleinmann et al. (1981) classify the star as a carbon star, apparently based on an unpublished *detection* of the $3.1 \mu\text{m}$ feature.

As a conclusion we find HCN/CO ratios consistent with the borderline value for carbon stars suggested by Bujarrabal et al. (1994a,b) in four stars, and two cases, that are almost certainly carbon stars, where the HCN/CO ratio is below the borderline value. In these cases confirmation of the HCN/CO ratio is desirable, since the HCN lines are generally weak or the estimated CO intensities are uncertain due to interstellar contamination. Another aspect of the apparent discrepancy may lie in the fact that the line ratios (HCN/CO and others) in Bujarrabal et al. (1994a,b) to discriminate O-, S- and C-stars are derived for IRAM data, while our ratios are derived from SEST data. In the larger beam of the SEST a different region of excitation may be sampled (in particular for the CO, since the HCN shell will in most cases be smaller than the size of the IRAM beam at 89 GHz) and therefore the 'critical lines ratios' derived for IRAM may not be applicable to SEST data.

Table 3. The $^{12}\text{C}/^{13}\text{C}$ ratio

Identification	1-0	2-1	3-2
RU Vir	>9.9	>16.5	-
17446–4048	>8.7	-	-
AFGL 2118	>5.9	>9.8	-
U Cyg	>5.9	>5.7	-
AFGL 67	>19.6	>18.0	>11.8
AFGL 190	>16.8	>22.2	-
IRC +50 096	>13.3	>15.8	>8.3
AFGL 865	>14.9	>11.6	-
CW Leo	>10.2	>6.9	>7.1
CIT 6	17.3	>13.9	>9.2
V Hya	>8.3	>3.2	-
Y CVn	>2.3	>3.8	-
RY Dra	>1.5	>3.9	-
AFGL 1922	>8.8	>9.0	-
V Aql	>7.3	>18.7	-
AFGL 2477	>6.9	>7.6	-
AFGL 2494	>39.4	>53.5	>12.4
S Cep	>11.9	>14.7	-
AFGL 3068	>7.1	>4.7	>3.7
LP And	>9.6	>9.3	>8.5

Notes. The $^{12}\text{C}/^{13}\text{C}$ ratio based on the integrated intensities of the J = 1-0, 2-1 and 3-2 lines, respectively.

4.3. The $^{12}\text{C}/^{13}\text{C}$ ratios

In Table 3 we have collected the $^{12}\text{CO}/^{13}\text{CO}$ ratio for the stars with ^{13}CO data. All ratios, except one, are lower limits, either because we only have upper limits to the ^{13}CO integrated intensities or because the parabolic line shapes of the ^{12}CO line profiles indicate that these lines are optically thick. Only in the case of CIT6 we derive a definite value for the $^{12}\text{CO}/^{13}\text{CO}$ ratio of about 17 based on the J = 1-0 line. That optical depth effects play a role even in this case is clear from a comparison with Kahane et al. (1992). They find a similar ratio of 13 for the ratio of the $^{12}\text{CO}/^{13}\text{CO}$ integrated 1-0 intensity but derive from model calculations a true $^{12}\text{CO}/^{13}\text{CO}$ ratio of 31.

4.4. The expansion velocities

The expansion velocities, derived as half the width at zero intensity, range from ~ 10 (Y CVn) to 31 km s^{-1} (V414 Per). The mean velocity of the sample is 18.2 km s^{-1} and 70% of the stars have velocities between 14 and 24 km s^{-1} .

Barnbaum et al. (1991) extended earlier work to show that stars with expansion velocities $\geq 17.5 \text{ km s}^{-1}$ are confined to galactic latitudes within 20 degrees of the plane. This correlation holds for all stars in our sample except two. One is a marginal case: CIT6 has $v_{\infty} = 17.6 \text{ km s}^{-1}$ and is located at $b = 56^\circ$, the other is the well-known object V Hya, which has a bipolar outflow (see Sect. 4.1.11).

4.5. The mass loss rates

Mass loss rates are calculated for the stars in the new sample; mass loss rates for the stars in the well-known sample can be

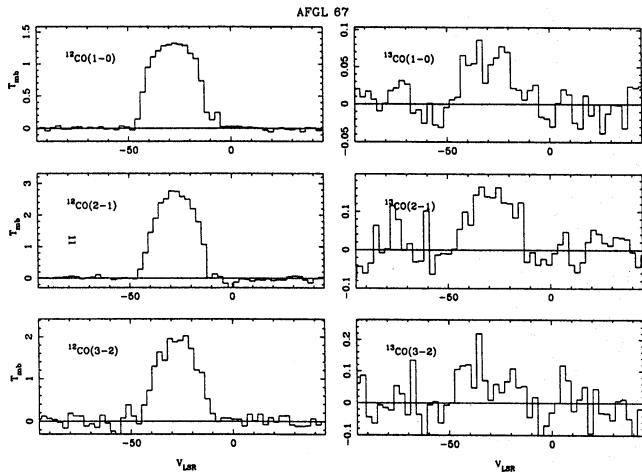


Fig. 15. AFGL 67

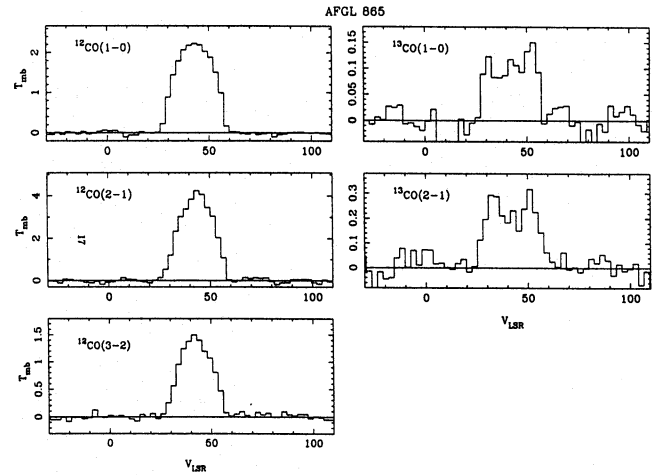


Fig. 18. AFGL 865

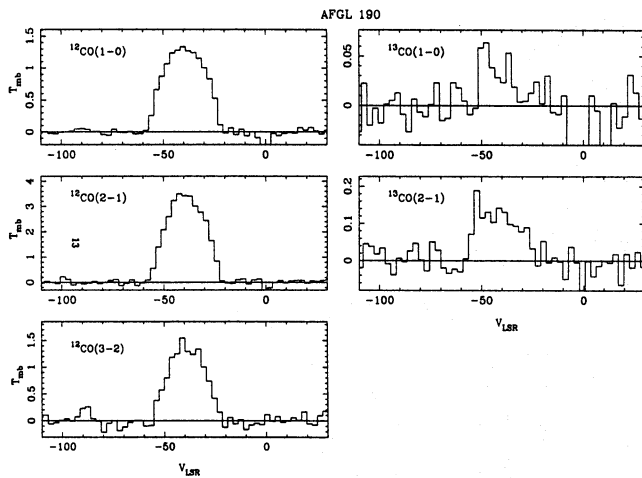


Fig. 16. AFGL 190

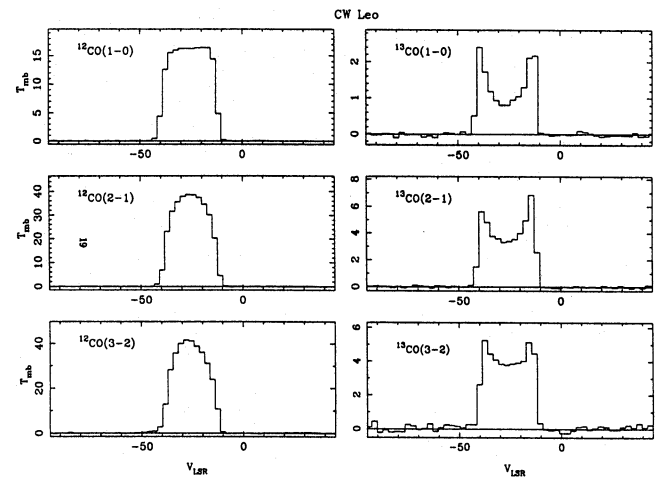


Fig. 19. CW Leo

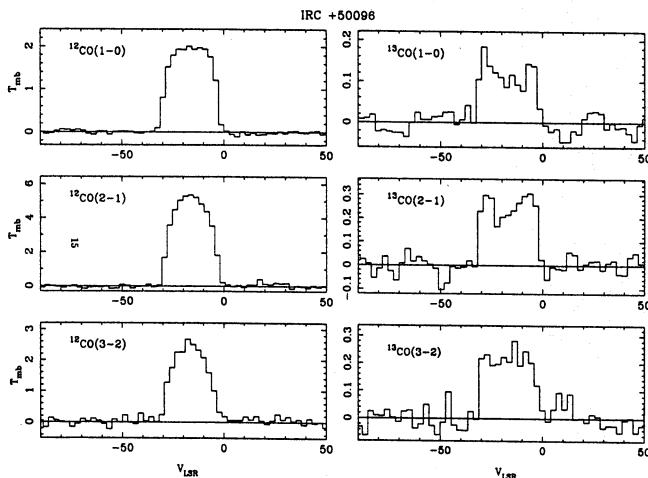


Fig. 17. IRC +50 096

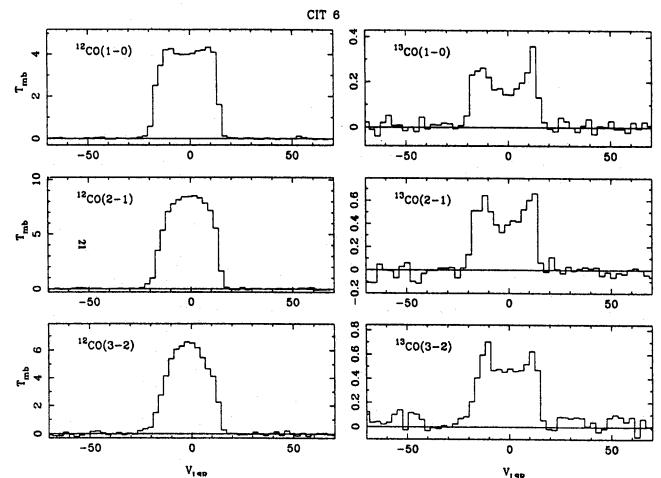


Fig. 20. CIT 6

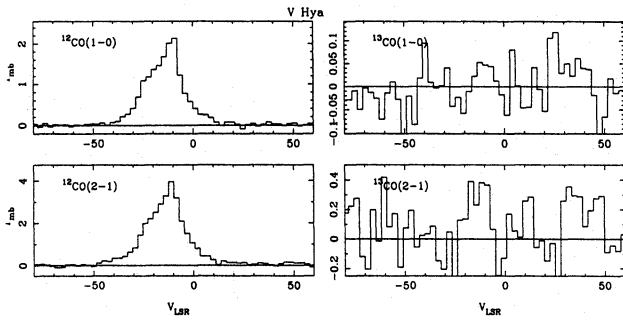


Fig. 21. V Hya

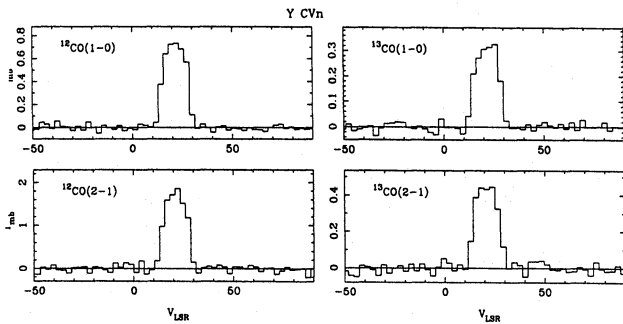


Fig. 22. Y CVn

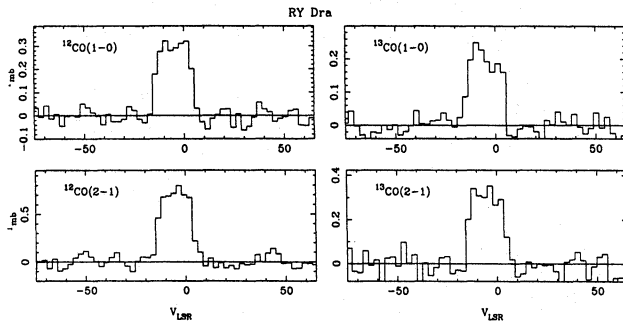


Fig. 23. RY Dra

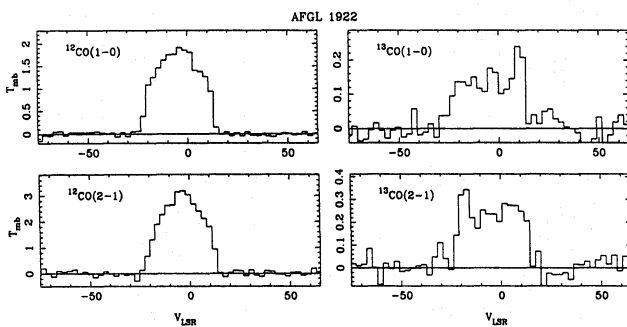


Fig. 24. AFGL 1922

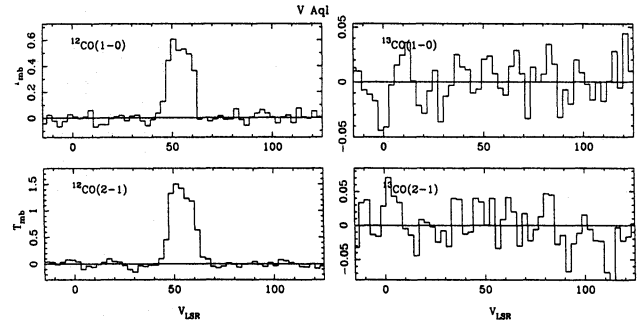


Fig. 25. V Aql

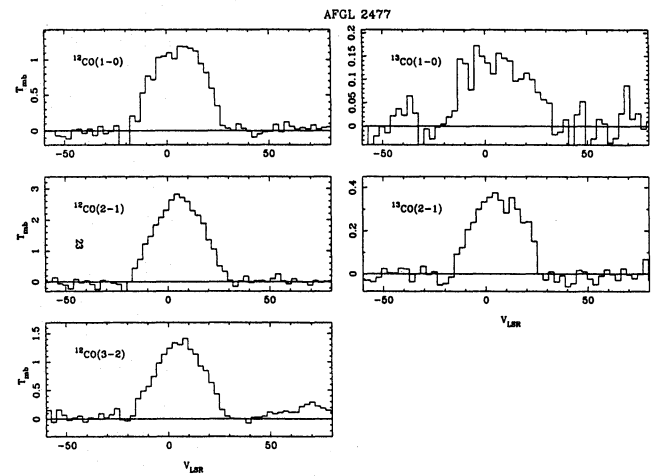


Fig. 26. AFGL 2477

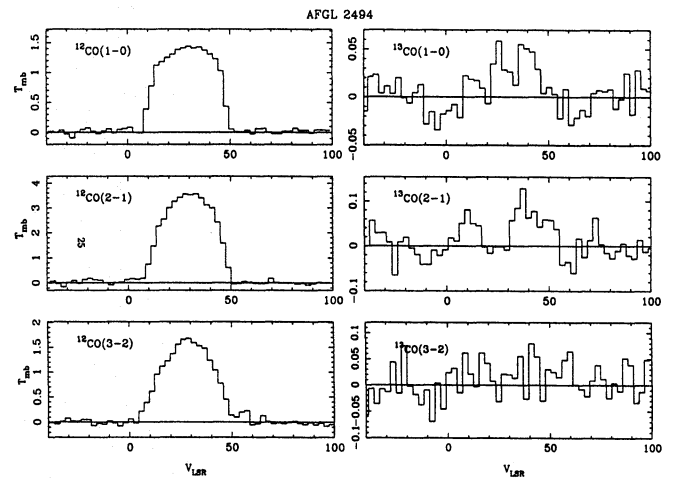


Fig. 27. AFGL 2494

Table 4. Mass loss rates for the new sample

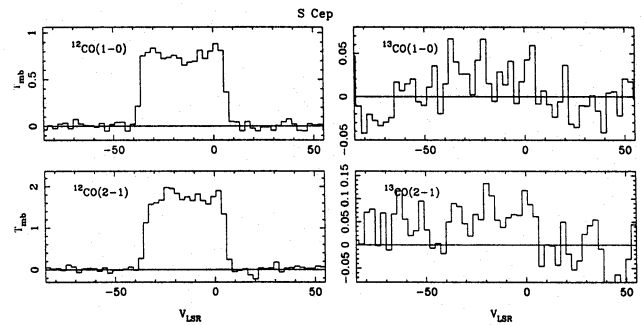
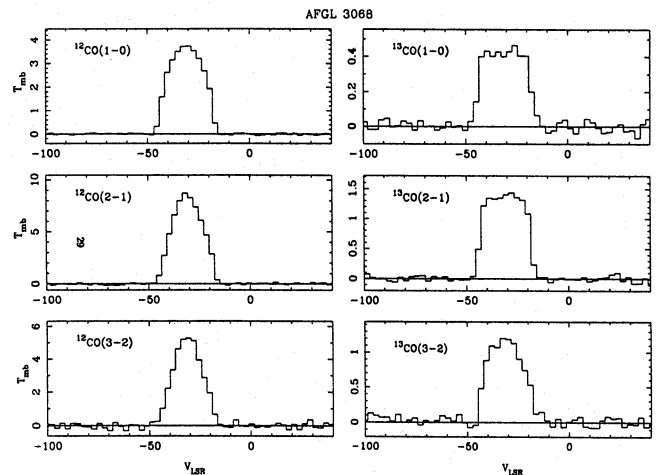
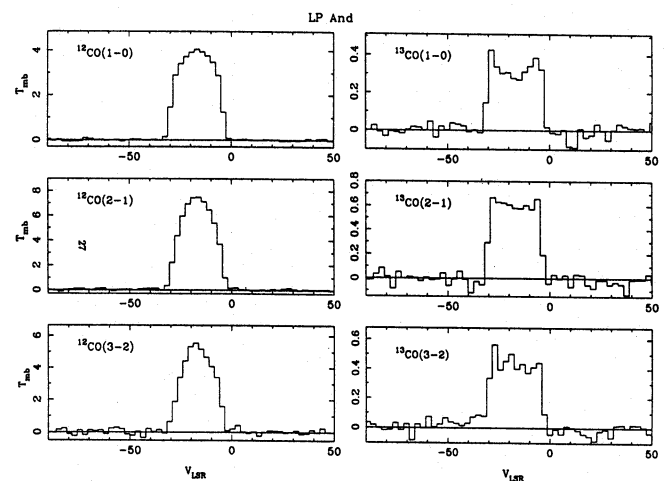
Identification	the mass loss rate at 1 kpc (in $10^{-6} M_{\odot} \text{yr}^{-1} \text{kpc}^{-2}$)			
	(1)	(2)	(3)	(4)
V414 Per	2.4	5.5	2.0	1.6
V636 Mon	4.2	8.4	3.2	1.3
AFGL 1085	3.2	-	2.9	3.1
07373-4021	-	6.4	-	1.5
AFGL 4078	6.1	15.5	3.6	6.0
08074-3615	5.2	-	3.9	4.9
09513-5324	8.0	4.3	5.3	2.8
11145-6534	3.9	-	2.5	3.0
11318-7256	6.8	9.0	5.5	4.1
12419-6058	3.7	-	3.1	2.6
RU Vir	1.9	3.8	1.2	1.4
AFGL 4183	5.9	3.7	4.0	2.8
AFGL 4202	10.9	10.9	6.4	8.2
16079-4812	3.9	4.7	2.6	2.6
17446-4048	8.2	5.3	4.9	2.5
AFGL 5416	4.2	8.5	3.1	9.0
AFGL 5440	8.3	6.0	4.3	3.1
18041-3317	2.1	-	1.9	0.84
AFGL 2096	0.71	1.4	0.57	1.9
AFGL 2118	1.6	2.3	1.2	1.0
AFGL 2154	13.0	6.5	9.2	5.8
AFGL 2256	1.5	-	1.8	1.9
AFGL 2333	5.3	8.1	2.8	7.0
AFGL 2513	4.5	6.8	2.9	4.2
U Cyg	0.91	1.7	0.57	0.81
AFGL 2604	0.38	1.1	0.30	1.0

Notes. (1) Mass loss rate from the $J = 1-0$ line and the formula in Olofsson et al. (1993a); (2) Mass loss rate from the $J = 2-1$ line and the formula in Olofsson et al. (1993a); (3) Mass loss rate based on the $J = 1-0$ line and the formula in Kastner (1992); (4) Mass loss rate based on the IRAS $60 \mu\text{m}$ flux and the formula in Jura (1987), assuming a gas-to-dust ratio of 200, a luminosity of $7050 L_{\odot}$, a dust opacity of $150 \text{ cm}^2 \text{ gr}^{-1}$ at $60 \mu\text{m}$ and a peak of the spectral energy distribution occurring at $3 \mu\text{m}$.

found in L93. Furthermore, a detailed analysis of both the spectral energy distributions and CO line profiles of the stars in the well-known sample is the subject of a future publication.

The mass loss rates (scaled to a distance of 1 kpc) are calculated from both the CO and infrared properties. For the mass loss rates based on the CO lines we used Eq. (2) of Olofsson et al. (1993a) which is applied to the 1-0 and 2-1 line separately, and Eq. (20) of Kastner (1992) for the 1-0 line. The mass loss rates based on the IRAS $60 \mu\text{m}$ flux-densities are calculated from the formula in Jura (1987), assuming for all objects a gas-to-dust ratio of 200, a luminosity of $7050 L_{\odot}$ (the mean luminosity of carbon stars in the LMC; see e.g. Groenewegen & de Jong 1993), a dust opacity at $60 \mu\text{m}$ of $150 \text{ cm}^2 \text{ gr}^{-1}$ and a peak of the spectral energy distribution occurring at $3 \mu\text{m}$. The mass loss rates are listed in Table 4.

The mass loss rates based on the 1-0 line from the formulae of Olofsson et al. (1993a) and Kastner (1992) are in good agreement. The average ratio is 1.42 with a maximum of 1.83 and a

**Fig. 28.** S Cep**Fig. 29.** AFGL 3068**Fig. 30.** LP And

minimum of 0.83. The formula of Olofsson et al. was corrected for the presence of helium, while Kastner's formula apparently was not. If this effect is taken into account the average ratio of the mass loss rates based on the two methods is 1.0. The ratio of the mass loss rates based on the 2-1 line to the 1-0 line is 1.32 with a maximum ratio of 2.89 and a minimum ratio 0.5. The ratio of the mass loss rates based on the 1-0 line and the formula of Olofsson et al. and the mass loss rate based on the $60\ \mu\text{m}$ flux is 1.30 with a maximum ratio of 3.3 and a minimum ratio of 0.37.

The different approaches indicate that in a statistical sense they give the same mass loss rates within 30%, but that mass loss rates for individual objects derived by these methods are uncertain by a factor of 3.

Acknowledgements. We thank J.-Y. Hu for observing four sources with the SEST during his observing run. This research has made use of the SIMBAD database, operated at CDS, Strasbourg, France. We thank the referee, V. Bujarrabal, for constructive comments. The observations were performed when MG was at the Astronomical Institute 'Anton Pannekoek' of the University of Amsterdam supported under grant 782-373-030 by the Netherlands Foundation for Research in Astronomy (ASTRON), which is financially supported by the Netherlands Organization for Scientific Research (NWO).

References

- Allen D.A., et al., 1977, ApJ 217, 108
 Avery L.W., et al., 1992, ApJS 83, 363
 Barnbaum C., Kastner J.H., Zuckerman B., 1991, AJ 102, 289
 Bujarrabal V., Fuente A., Omont A., 1994a, ApJ 421, L47
 Bujarrabal V., Fuente A., Omont A., 1994b, A&A 285, 247
 Charbonnel C., 1994, A&A 282, 811
 Dame T.M., et al., 1987, ApJ 322, 706 (D87)
 Deguchi S., Nakada Y., Forster J.R., 1989, MNRAS 239, 825
 Epchtein N., Le Bertre T., Lépine J.R.D., 1990, A&A 227, 82
 Forveille T., Guilloteau S., Lucas R., 1990, IRAM publication
 Fuenmayor F.J., 1981, Rev. Mexicana. Astron. Astrof. 6, 83
 Gaylard M.J., West M.E., Whitelock P.A., Cohen R.J., 1989, MNRAS 236, 247
 Grasdalen G.L., Gehrz R.D., Hackwell J.A., Castelaz M., Gullixson C., ApJS 53, 413
 Groenewegen M.A.T., de Jong T., van der Blik N.S., Slijkhuis S., Willems F.J., 1992, A&A 253, 150
 Groenewegen M.A.T., de Jong T., 1993, A&A 267, 410
 Groenewegen M.A.T., 1994, A&A 290, 544
 Groenewegen M.A.T., de Jong T., Geballe T.R., 1994, A&A 287, 163
 Groesbeek T.D., Phillips T.G., Blake G.A., 1994, ApJS 94, 147
 Haikala L.K., 1990, A&AS 85, 875
 Hall P.J., Allen D.A., Troup E.R., Wark R.M., Wright A.E., 1990, MNRAS 243, 480
 Joyce R.R., et al., 1977, ApJ 213, L125
 Jura M., 1987, ApJ 313, 743
 Jura M., Kahane C., Omont A., 1988, A&A 201, 80
 Kahane C., Audinos P., Barnbaum C., Morris M., 1993, in: "Mass loss on the AGB and beyond", ed. H. Schwarz, ESO, p. 437
 Kahane C., Cernicharo J., Gómez-González J., Guélin M., 1992, A&A 256, 235
 Kahane C., Maizels C., Jura M., 1988, ApJ 328, L25
 Kastner J.H., 1992, ApJ 401, 337
 Kleinmann S.G., Gillett F.C., Joyce R.R., 1981, ARA&A 19, 411
 Knapp G.R., Chang K.M., 1985, ApJ 293, 281
 Knapp G.R., Morris M., 1985, ApJ 292, 640
 Le Squeren A.M., Sivagnanam P., Dennefeld M., David P., 1992, A&A 254, 133
 Loup C., Forveille T., Omont A., Paul J.F., 1993, A&AS 99, 291 (L93)
 Lucas R., Guilloteau S., Omont A., 1988, A&A 194, 230
 Mauersberger R., Guélin M., Martin-Pintado J., Thum C., Cernicharo J., Hein H., Navarro S., 1989, A&AS 79, 217
 Nyman L.-A., et al., 1992, A&AS 93, 121
 Olofsson H., 1993, in: "Mass loss on the AGB and beyond", ed. H. Schwarz, ESO, p. 330
 Olofsson H., Eriksson K., Gustafsson B., Carlstöm U., 1993a, ApJS 87, 267
 Olofsson H., Eriksson K., Gustafsson B., Carlstöm U., 1993b, ApJS 87, 305
 Omont A., et al., 1993, A&A 267, 515
 Sopka R.J., Olofsson H., Johansson L.E.B., Nguyen-Q-Rieu, Zuckerman B., 1989, A&A 210, 78
 te Lintel Hekkert P., Caswell J.L., Habing H.J., Haynes R.F., Norris R.P., 1990, A&AS 90, 327
 Tsuji T., et al., 1988, ApJ 327, L23
 Van der Veen W.E.C.J., Olofsson H., 1990, in: From Miras to Planetary Nebulae, eds. M.O. Mennessier, A. Omont, editions Frontières, Gif-sur-Yvette, p. 139
 Volk K., Kwok S., Langill P.P., 1992, ApJ 391, 285
 Volk K., Kwok S., Woodsworth A.W., 1993, ApJ 402, 292
 Williams P.G., White G.J., 1992, A&A 266, 365
 Woodsworth A.W., Kwok S., Chan S.J., Murowinski R., 1991, A&A 246, 447
 Zuckerman B., Dyck H.M., 1986a, ApJ 304, 394
 Zuckerman B., Dyck H.M., 1986b, ApJ 311, 345
 Zuckerman B., Dyck H.M., 1989, A&A 209, 119
 Zuckerman B., Dyck H.M., Claussen M.J., 1986, ApJ 304, 401

This article was processed by the author using Springer-Verlag L^AT_EX A&A style file version 3.